ceramics

MDPI

Article

Calcium Silicate Hydrate Cation-Exchanger from Paper Recycling Ash and Waste Container Glass

Andrew P. Hurt [1], Aimee A. Coleman [2], Haosen Ma [3], Qiu Li [3] and Nichola J. Coleman [1,*]

[1] School of Science, Faculty of Engineering and Science, University of Greenwich, Chatham Maritime, Kent ME4 4TB, UK; a.hurt@gre.ac.uk
[2] HH Wills Physics Laboratory, School of Physics, University of Bristol, Bristol BS8 1QU, UK; wy19042@bristol.ac.uk
[3] State Key Laboratory of Silicate Materials for Architectures, Wuhan University of Technology, Wuhan 430070, China; mahaosen@whut.edu.cn (H.M.); qiu-li@whut.edu.cn (Q.L.)
* Correspondence: n.coleman@gre.ac.uk; Tel.: +44-208-331-9825

Abstract: Synthetic 11 Å tobermorite ($Ca_5Si_6O_{16}(OH)_2.4H_2O$) and its Al-substituted analogue are layer-lattice ion-exchangers with potential applications in nuclear and hazardous wastewater treatment. The present study reports the facile one-pot hydrothermal synthesis of an Al-tobermorite-rich cation-exchanger from a combination of paper recycling ash, post-consumer container glass, and lime, with compositional ratios of [Ca]/[Si + Al] = 0.81 and [Al]/[Si + Al] = 0.18. The reaction products were characterized by powder X-ray diffraction analysis, ^{29}Si magic angle spinning nuclear magnetic resonance spectroscopy, and scanning electron microscopy. Hydrothermal processing in 4 M $NaOH_{(aq)}$ at 100 °C for 7 days yielded an Al-tobermorite-rich product that also contained katoite ($Ca_3Al_2SiO_{12}H_8$), portlandite ($Ca(OH)_2$), calcite ($CaCO_3$), and amorphous silicate gel. The hydrothermal product was found to have a Cs^+ cation exchange capacity of 59 ± 4 meq 100 g^{-1} and selective Cs^+ distribution coefficients (K_d) of 574 ± 13 and 658 ± 34 cm^3 g^{-1} from solutions with molar ratios [Cs^+]:[Na^+] and [Cs^+]:[Ca^{2+}] of 1:100. In a batch sorption study at 20 °C, the uptakes of Pb^{2+}, Cd^{2+}, and Cs^+ were determined to be 1.78 ± 0.04, 0.65 ± 0.06, and 0.36 ± 0.03 mmol g^{-1}, respectively. The kinetics of Pb^{2+}, Cd^{2+}, and Cs^+ removal were described by the pseudo-second-order rate model, which gave respective rate constants (k_2) of 0.010, 0.027, and 1.635 g $mmol^{-1}$ min^{-1}, and corresponding correlation coefficients (R^2) of 0.997, 0.996, and 0.999. The metal ion sorption properties of the tobermorite-rich product compared favorably with those of other waste-derived tobermorites reported in the literature. Potential strategies to improve the yield, crystallinity, and sorption characteristics of the product are discussed.

Keywords: tobermorite; waste glass; paper recycling ash; sorbent; ion-exchange; lead; cadmium; caesium

Citation: Hurt, A.P.; Coleman, A.A.; Ma, H.; Li, Q.; Coleman, N.J. Calcium Silicate Hydrate Cation-Exchanger from Paper Recycling Ash and Waste Container Glass. *Ceramics* **2022**, *5*, 301–317. https://doi.org/10.3390/ceramics5030024

Academic Editors: Philippe Blanchart, Cyriaque Rodrigue Kaze and Gisèle Laure Lecomte-Nana

Received: 29 June 2022
Accepted: 21 July 2022
Published: 22 July 2022

1. Introduction

11 Å tobermorite ($Ca_5Si_6O_{16}(OH)_2.4H_2O$) is a rare, naturally-occurring, layer-lattice ion-exchange mineral arising from the action of hydrothermal fluids on basic igneous rock [1]. It is the principal binder in autoclaved concrete and is also formed at the cement–rock interface in nuclear repositories, and by the interaction of seawater with Roman pozzolanic marine structures [2–6]. Synthetic tobermorite is readily prepared under alkaline hydrothermal conditions, typically between 100 and 200 °C, from a wide range of calcium- and silicate-bearing analytical grade reagents [7–11], rocks [12–15], and waste materials [16–42].

The 11 Å tobermorite structure comprises a double layer of calcium oxide polyhedra connected on both sides to wollastonite-like silicate chains running along the *b*-axis. These layers are stacked in the *c*-direction to give a (0 0 2) basal spacing in the range 11.2 to 11.7 Å [1]. This arrangement creates inter-layer channels that house labile, charge-balancing

cations, and water molecules. Structural defects arise from stacking imperfections, vacancies along the silicate chains, and the condensation of silicate tetrahedra between adjacent layers [25].

Compositional variations can be obtained during hydrothermal synthesis by the partial isomorphic replacement of SiO_4^{4-} for other tetrahedral oxyanions (e.g., AlO_4^{5-}, FeO_4^{5-}, PO_4^{3-}, SO_4^{2-}), by the limited substitution of structural Ca^{2+} for other divalent cations (e.g., Mg^{2+}), and by the complete replacement of structural Ca^{2+} with trivalent lanthanides (e.g., Eu^{3+}, Ce^{3+}, Sm^{3+}, Tb^{3+}) [43–49]. Extensive ion-exchange of the labile inter-layer cations for a wide range of mono-, di-, and trivalent species (e.g., Na^+, K^+, Cs^+, Ag^+, Sr^{2+}, Zn^{2+}, Cr^{3+} inter alia) can be achieved within a few hours and is generally accompanied by a change in basal spacing [9,27,32,35,36,50]. In contrast, post hoc exchange of structural Ca^{2+} for other di- and trivalent cations takes place over many days, generally causing structural disruption and progressive amorphization of the lattice [32,51–53].

Naturally occurring 11 Å tobermorite is insufficiently abundant to find any practical uses other than geological and chemical curiosity [1]. However, synthetic tobermorites are relevant to a wide range of industrial and technological applications including autoclaved cements, thermal insulating materials, waste management, catalysis, soil conditioning, and biomaterials [2,3,13–48].

In 2020, the European Declaration on Paper Recycling reported that 73.9% of the 75.8 Mt of paper and board consumed in Europe was recycled [54]. Europe had the highest continental paper recycling efficiency, followed by North America at 65.7%, with a global average of 58.6% [54]. Sludges generated from the de-inking and reprocessing of waste paper are commonly incinerated for the purposes of volume-reduction and energy-recovery [55]. The resulting paper recycling ash (PRA) contains potentially reactive calcium (alumino)silicate phases that can be exploited in the hydrothermal synthesis of tobermorite when stoichiometrically adjusted with additional silicate-bearing reagents [25,29,30,56].

While it is technically possible to recycle up to 90% of waste soda-lime-silica container glass (WCG), in practice, this target is undermined by various geographical, infrastructural, and economic factors [57–59]. Accordingly, approximately 200 Mt of post-consumer container glass is currently landfilled per annum [56]. Many studies have been carried out to upcycle this WCG into value-added products such as sorbents, ion-exchangers, catalysts, ceramics, geopolymers, and construction materials [57,59–65]. WCG has also been used as a feedstock for the preparation of tobermorite in alkaline media [17–21,39].

The present study considered the feasibility of a simple one-pot synthesis of 11 Å tobermorite from a combination of PRA, WCG, and lime under alkaline hydrothermal conditions at 100 °C. Reaction products were characterized by powder X-ray diffraction analysis (XRD), ^{29}Si magic angle spinning nuclear magnetic resonance spectroscopy (MAS NMR), and scanning electron microscopy (SEM). This study also evaluated the Cs^+ cation exchange capacity (CEC), the selective Cs^+ distribution coefficients (K_d) from solutions with molar ratios of $[Cs^+]$:$[Na^+]$ or $[Cs^+]$:$[Ca^{2+}]$ equal to 1:100, and the uptake kinetics of aqueous Pb^{2+}, Cd^{2+}, and Cs^+ ions by the waste-derived hydrothermal product.

2. Materials and Methods

2.1. Materials

Paper recycling ash (PRA) was obtained from Aylesford Newsprint, Kent, UK, and ground in an agate mill to pass 250 μm. Clear flint waste container glass (WCG) was collected from the municipal refuse in Rochester, Kent, UK, rinsed with tap water to remove labels, dried, and milled to pass 250 μm. Quantitative elemental analyses of the PRA and WCG were obtained by X-ray fluorescence spectroscopy using a Bruker S2 PUMA Series 2 spectrometer (Bruker AXS, Karlsruhe, Germany) and are listed in Table 1 as oxide conversions. PRA and WCG were also characterized by X-ray diffraction using a Siemens Kristalloflex 810 diffractometer (Bruker AXS, Karlsruhe, Germany).

Table 1. Compositions of paper recycling ash (PRA) and waste container glass (WCG).

Oxide	PRA (wt%)	WCG (wt%)
SiO_2	30.4	72.50
Na_2O	0.23	13.22
CaO	41.3	11.11
Al_2O_3	18.6	1.31
MgO	3.84	0.96
TiO_2	0.64	0.05
K_2O	0.52	0.44
P_2O_5	0.34	-
Fe_2O_3	0.86	0.10
WO_3	0.33	-
SO_3	0.98	018
Cr_2O_3	0.01	-
Loss on ignition	2.26	-

All other analytical grade reagents (i.e., NaOH, NaCl, KCl, CaO, $CaCl_2$, $Pb(NO_3)_2$, $Cd(NO_3)_2.4H_2O$, CsCl, and 1000 ppm atomic absorption standards) were obtained from Sigma-Aldrich, Gillingham, UK, and used without further modification.

2.2. Hydrothermal Synthesis and Characterization

The 11 Å tobermorite samples were prepared in triplicate by dry blending 3.5 g of PRA, 3.5 g of WCG, and 1.5 g of CaO prior to mixing with 60 cm^3 of 4 M $NaOH_{(aq)}$, sealing in a poly(tetrafluoroethylene) autoclave, and heating at 100 °C for 1, 2, or 7 days (viz. TOB-1, TOB-2, and TOB-7). The selected combination of reagents gave the following molar ratios, which are theoretically appropriate for the production of Al-substituted 11 Å tobermorite: [Ca]/[Si+Al] = 0.81 and [Al]/[Si+Al] = 0.18 [29]. The solid products were separated from the reaction liquor by gravitational filtration, washed to pH ~8 with deionized water, and dried in air at 60 °C prior to characterization by powder X-ray diffraction analysis (XRD) and scanning electron microscopy (SEM). Secondary electron images of the products were acquired from uncoated samples attached to carbon tabs on an Hitachi SU8030 scanning electron microscope (Hitachi, Tokyo, Japan) with an accelerating voltage of 1 kV.

Powder XRD data were obtained using a Siemens Kristalloflex 810 diffractometer (Bruker AXS, Karlsruhe, Germany) with a Cu Kα 1.5406 source, a step size of 0.019° in the 2θ range from 2 to 60°, and a measuring time of 1 s per step. The degree of crystallinity was estimated from the ratio of the area of the crystalline peaks to the total area of the pattern using Bruker EVA version 5.1 software (Bruker AXS, Karlsruhe, Germany). The identification of the phases, 11 Å tobermorite (PDF® 00-019-0052), katoite (PDF® 00-038-0368), portlandite (PDF® 01-070-5492), calcite (PDF® 01-078-3262), gehlenite (PDF® 00-020-0199), åkermanite (PDF® 01-074-0990), β-dicalcium silicate (PDF® 00-003-0761), and anorthite (PDF® 01-070-0287) was carried out using ICDD Powder Diffraction Files™.

It should be noted that, in this manuscript, the names of naturally occurring minerals were appropriated for the description of their synthetic counterparts. The formulae assigned to the synthetic phases are those given in the corresponding PDF® files.

The weight fractions of the crystalline phases were obtained by Rietveld refinement using Bruker TOPAS version 5.1 software (Bruker AXS, Karlsruhe, Germany) [66]. The background was calculated with a Chebyshev polynomial function and profiles were fitted using structural data from the Inorganic Crystal Structure Database (FIZ, Karlsruhe, Germany). The unit cell parameters and crystallite sizes were refined, while the atomic positions and atomic displacement parameters were fixed. The preferred orientation of tobermorite was accounted for by using a spherical harmonics function. Examples of the phase identification and refinement are given in Figures A1 and A2 in Appendix A.

A single pulse ^{29}Si MAS NMR spectrum of TOB-7 was collected on a JEOL JNMECX 300 MHz spectrometer (JEOL (UK) Ltd., Welwyn Garden City, UK) with a pulse delay of 60 s, an acquisition time of 0.229 s, and 6000 scans. ^{29}Si chemical shifts were referenced

to tetramethylsilane (TMS). The free induction decay profiles were processed by Delta software (provided by JEOL) to obtain spectra that were then analyzed using Igor Pro software (WaveMetrics Inc., Portland, OR, USA).

The notation used to describe the silicate structures of tobermorites is such that the symbol Q denotes one SiO_4^{4-} tetrahedron and a superscript indicates the number of other Q units to which it is bonded. Substitution by an AlO_4^{5-} unit is indicated in parentheses, for example, a mid-chain SiO_4^{4-} unit bonded between one SiO_4^{4-} unit and one AlO_4^{5-} unit is represented as $Q^2(1Al)$. The yield, mean chain length (MCL), and Al:Si ratio of the tobermorite product were estimated from the deconvoluted ^{29}Si MAS NMR spectrum using the following relationships [67]:

$$\text{Tobermorite yield} = [(\Sigma Q^n - (\Sigma Q^3 + \Sigma Q^4)) \times 100]/\Sigma Q^n \quad (1)$$

$$\text{MCL} = 2[(Q^1 + Q^2 + {}^3/_2(Q^2(1Al) + Q^3(1Al))]/Q^1 \quad (2)$$

$$\text{Al:Si ratio} = [{}^1/_2(Q^2(1Al) + {}^1/_3Q^3(1Al)]/[Q^1 + Q^2 + Q^2(1Al) + Q^3(1Al)] \quad (3)$$

where ΣQ^n represents the sum of the intensities of all of the silicate resonances.

2.3. Cation Exchange Capacity and Cs^+ Selectivity of TOB-7

Methods reported by Komarneni et al. [68–70] were used, in triplicate, to determine the cation exchange capacity (CEC) and Cs^+ selectivity of the 7-day tobermorite-bearing hydrothermal product (TOB-7) at 20 °C. In brief, for the determination of CEC, the ion-exchange sites of 0.100 g of the sample were saturated with K^+ ions by repeated equilibration with 0.1 M $KCl_{(aq)}$ solutions. The K^+ ions were subsequently displaced with Cs^+ ions by four consecutive washings with 0.01 M $CsCl_{(aq)}$, which were then combined and analyzed for K^+ by atomic emission spectrophotometry [30].

For the measurement of Cs^+ selectivity, approximately 0.08 g of accurately weighed tobermorite sample were contacted with 40 cm^3 of 0.02 M $NaCl_{(aq)}$ or 0.02 M $CaCl_{2(aq)}$ containing 2×10^{-4} M $CsCl_{(aq)}$ (i.e., solutions having molar ratios $[Cs^+]$:$[Na^+]$ and $[Cs^+]$:$[Ca^{2+}]$ equal to 1:100). Following equilibration for 24 h at 22 °C, the supernatant liquor was recovered and analyzed for Cs^+ by atomic emission spectrophotometry [30]. The distribution coefficient, K_d, a measure of Cs^+ selectivity, was then calculated as the ratio of the amount of Cs^+ sorbed per gram of tobermorite sample to the amount of Cs^+ remaining per cubic centimeter of solution.

2.4. Kinetics of Sorption of Pb^{2+}, Cd^{2+}, and Cs^+ by TOB-7

The uptake kinetics of Pb^{2+}, Cd^{2+}, and Cs^+ by the 7-day hydrothermal product, TOB-7, were determined, in triplicate, by contacting 50 mg of TOB-7 with 200 cm^3 of 0.5 mM metal nitrate solution for up to 24 h at 20 °C. After 0.5, 1, 2, 3, 6, 9, and 24 h, the pH values of the supernatant liquors were recorded, and 2.0 cm^3 aliquots were removed for quantitative analysis by inductively coupled plasma optical emission spectroscopy (ICP-OES) using a TJA Iris simultaneous ICP-OES spectrometer (TJA, MA, USA).

The Pb^{2+}, Cd^{2+}, and Cs^+ uptake data were analyzed using the pseudo-first- and pseudo-second-order rate models [18,20,36]. The linear form of the pseudo-first-order rate equation describes processes in which the reaction rate is proportional to the number of available sorption sites, and is given by the following relationship [18,20,36]:

$$\log(q_e - q_t) = \log q_e - k_1 t/2.303 \quad (4)$$

where k_1 (in min^{-1}) is the pseudo-first-order rate constant; q_t (in mmol g^{-1}) is the extent of sorption at time t (in min); and q_e (in mmol g^{-1}) is the extent of sorption at equilibrium. This rate equation is relevant when a linear relationship exists between $\log(q_e - q_t)$ and t, in which case k_1 can be estimated from the gradient of the plot.

The pseudo-second-order rate model describes sorption processes in which the reaction rate is proportional to the square of the number of available sorption sites, and can be expressed by the following [18,20,36]:

$$t/q_t = 1/k_2 q_e^2 + t/q_e \quad (5)$$

where k_2 (in g mmol^{-1} min^{-1}) is the pseudo-second-order rate constant. Estimates of k_2 and q_e can be obtained from the intercept and gradient of a linear plot of t/q_t against t.

3. Results

3.1. Characterization of PRA, WCG, and the Hydrothermal Products

Powder XRD data for PRA and WCG are depicted in Figure 1. WCG was amorphous and the crystalline phases of PRA were found to be gehlenite ($Ca_2Al_2SiO_7$), åkermanite ($Ca_2MgSi_2O_7$), β-dicalcium silicate (Ca_2SiO_4), and anorthite ($CaAl_2Si_2O_8$) (Figure 1).

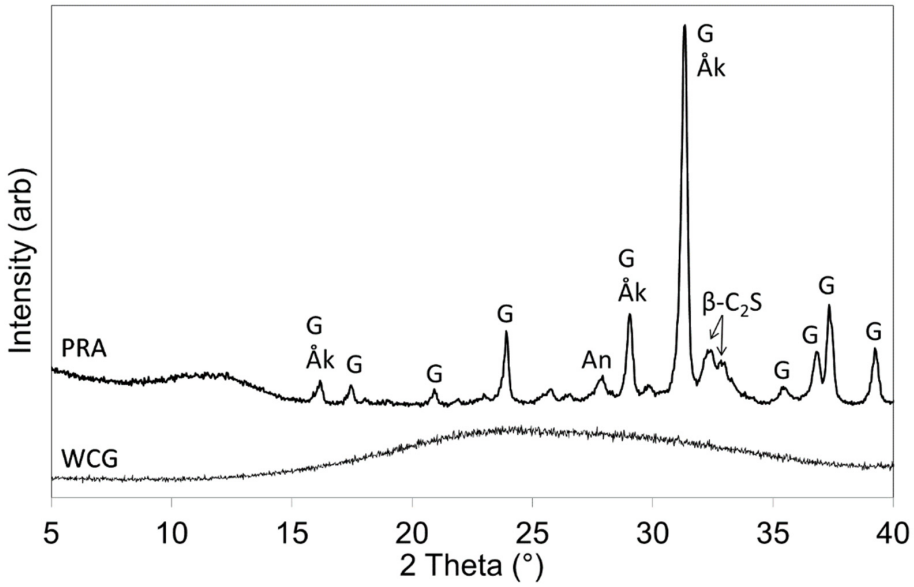

Figure 1. XRD patterns of WCG and PRA (Key: Åk = åkermanite; An = anorthite; β-C2S = β-dicalcium silicate; G = gehlenite).

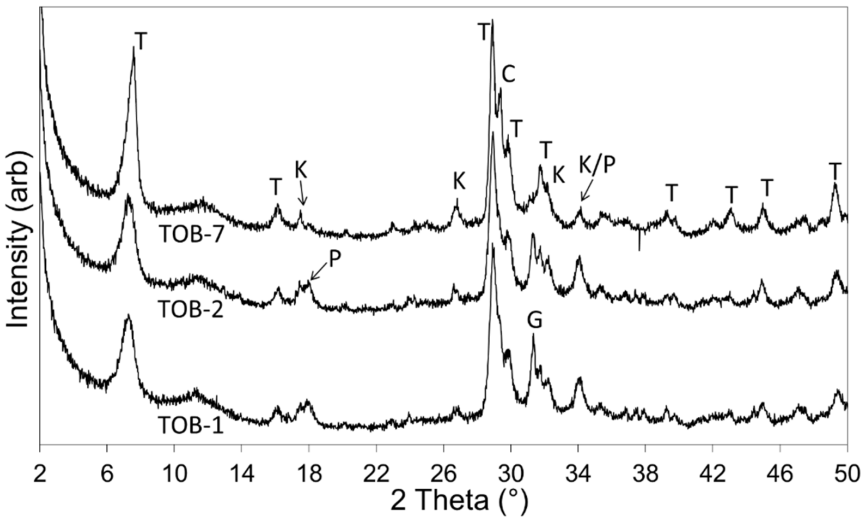

Figure 2. XRD patterns of 1-, 2-, and 7-day hydrothermal products (viz. TOB-1, TOB-2, and TOB-7) (Key: C = calcite; G = gehlenite; K = katoite; P = portlandite; T = Al-tobermorite).

Powder XRD data for the 1-, 2- and 7-day products of hydrothermal reaction between paper recycling ash, waste container glass, and lime in 4 M sodium hydroxide solution are shown in Figure 2. The Rietveld refinement data are listed in Table 2 and the quantities of the constituent phases are illustrated in Figure 3.

Table 2. Compositions of the hydrothermal products.

Component	TOB-1	TOB-2	TOB-7
Tobermorite (wt%) (PDF® 00-019-0052)	36.7	37.6	50.3
Katoite (wt%) (PDF® 00-038-0368)	3.7	5.0	6.1
Portlandite (wt%) (PDF® 01-070-5492)	5.9	6.3	2.5
Calcite (wt%) (PDF® 01-078-3262)	3.6	2.6	7.8
Gehlenite (wt%) (PDF® 00-020-0199)	6.6	6.0	-
Amorphous content (wt%)	43.5	42.5	33.3
Weighted profile R-factor (R_{wp})	18.5	18.3	25.7
Goodness of fit (GOF)	1.8	1.8	2.7

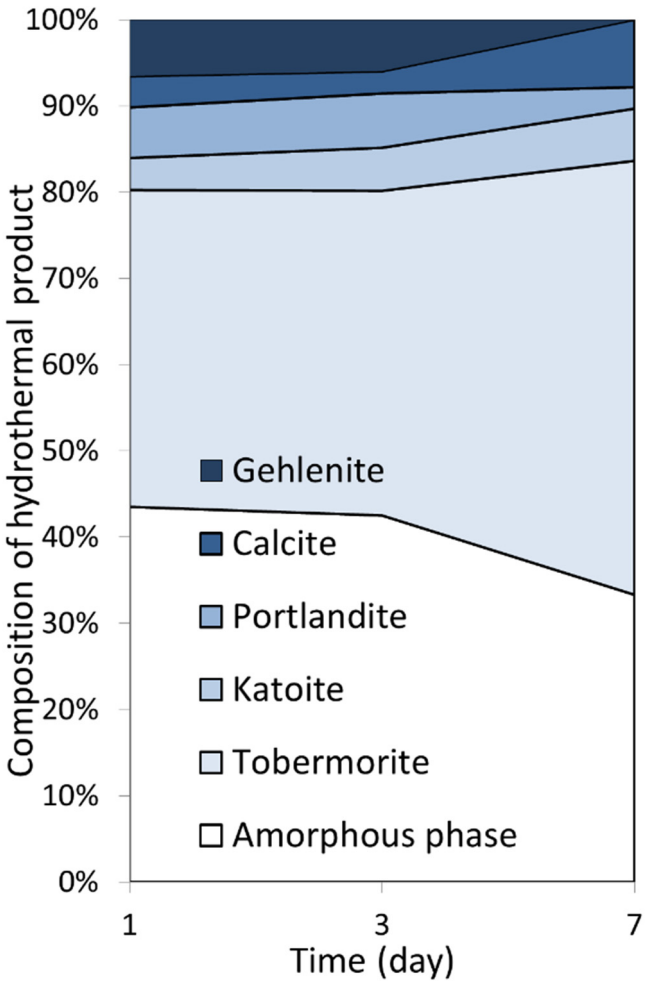

Figure 3. Compositions of the 1-, 2-, and 7-day hydrothermal products.

XRD analysis indicated that the åkermanite, β-dicalcium silicate, and anorthite phases of the PRA reagent were consumed within one day at 100 °C in 4 M sodium hydroxide

solution, and that gehlenite was comparatively less reactive with 6.6 wt% remaining in the sample (Table 2, Figure 3). After one day, the principal crystalline component of the hydrothermal product was Al-substituted 11 Å tobermorite at ~37 wt%, which continued to develop up to ~50 wt% within seven days. An overall increase in crystallinity from 56.5 wt% to 66.7 wt% was observed between one and seven days (Table 2). Within this timeframe, all of the residual gehlenite had reacted and the minor phases present in the product were observed to be the hydrogarnet, katoite, portlandite (arising from the hydration of the lime reagent), and calcite (resulting from atmospheric carbonation) (Table 2, Figure 3).

The deconvoluted ^{29}Si MAS NMR spectrum of the 7-day hydrothermal product, TOB-7, is shown in Figure 4 and estimates of the relative abundance of Q^n species, tobermorite-content, mean chain length (MCL), and Al:Si ratio of the silicate system of the tobermorite lattice are listed in Table 3. The spectrum comprises signals arising from Q^1 chain-end and dimeric silicate species at −79.1 ppm, Q^2 and Q^2(1Al) mid-chain tetrahedra at −85.0 and −81.9 ppm, respectively, and branching Q^3(1Al) species at −91.2 ppm [67]. The very broad signals centered at approximately −98 ppm and −107 ppm arise from amorphous calcium (alumino)silicate gel, which accounts for approximately a quarter of the silicate species present in the sample.

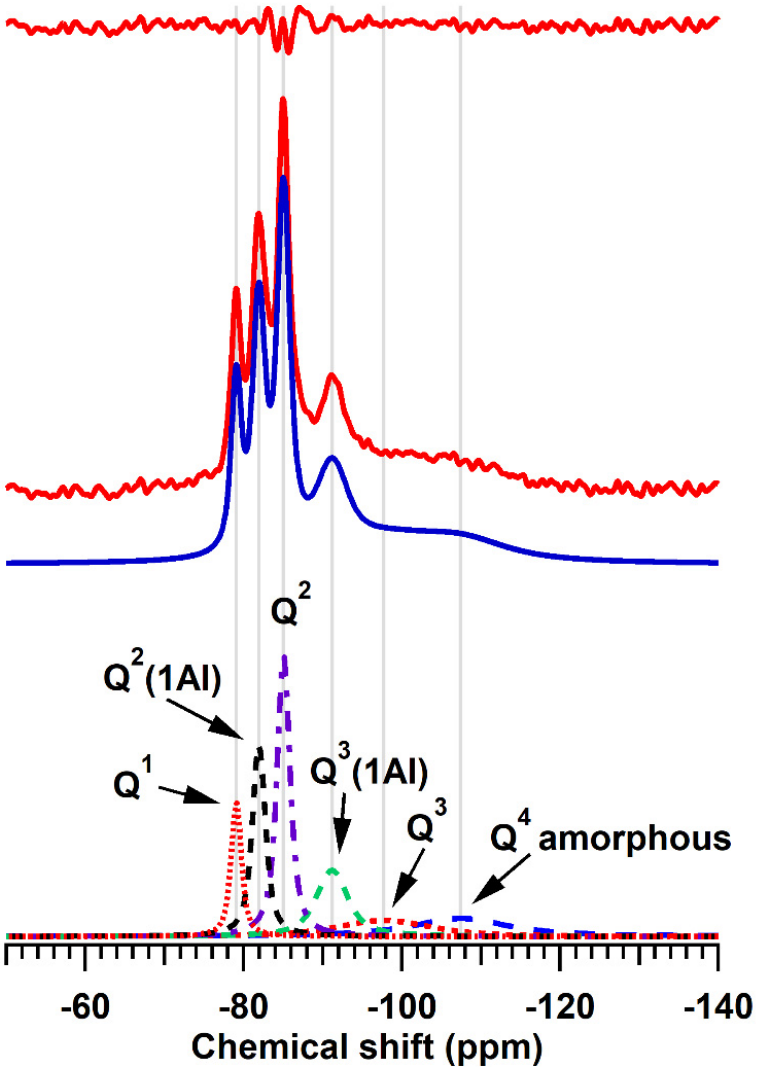

Figure 4. ^{29}Si MAS NMR spectrum of product TOB-7. The experimental and calculated spectra are depicted, respectively, as continuous red and blue lines. The individually resolved resonances are presented as dashed lines and the residual between the calculated and experimental spectra is shown in red at the top of the figure.

Table 3. Relative abundance of Q^n species and their chemical shifts, amorphous-content, mean aluminosilicate chain length (MCL), and Al:Si ratio of tobermorite in TOB-7.

Parameter	Chemical Shift (ppm)	Quantity
Q^1	−79.1	10.6%
Q^2(1Al)	−81.9	19.6%
Q^2	−85.0	28.6%
Q^3(1Al)	−91.2	15.9%
Q^3	−97.7	11.0%
Q^4	−107.4	14.3%
Amorphous-content	-	25.4%
MCL	-	8.74
Al:Si ratio	-	0.202

Secondary electron images of TOB-7 are shown in Figure 5 and indicate that the hydrothermal product presented as a highly textured granular material in the particle size range 5–10 µm. The characteristic reticular morphology of Al-substituted 11 Å tobermorite was seen to populate the entire surface of the granules, and no other crystalline phases were observed (Figure 5).

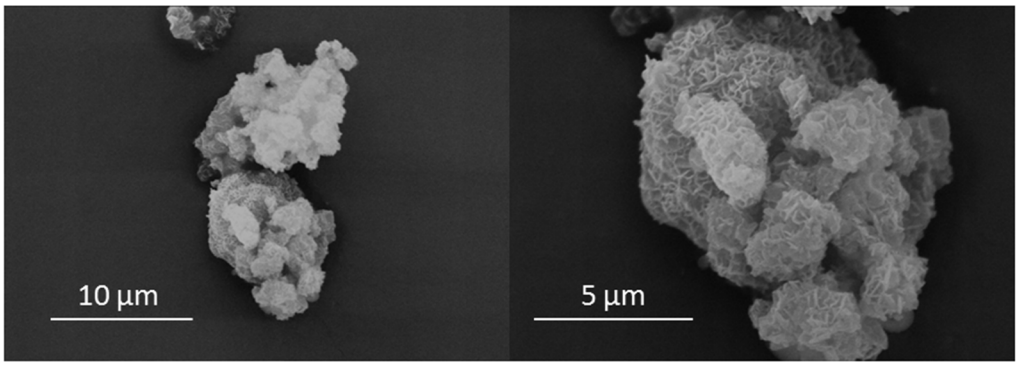

Figure 5. Secondary electron images of the 7-day hydrothermal product (TOB-7).

3.2. Cation Exchange Capacity and Cs^+ Selectivity

The Cs^+ for K^+ cation exchange capacity of TOB-7 was found to be 59 ± 4 meq 100 g^{-1} (i.e., 0.59 mmol g^{-1}, 32.5 mg g^{-1}). The 7-day hydrothermal product exhibited a preference for Cs^+ over Na^+ and Ca^{2+}, respectively removing 55 and 59% of Cs^+ ions from binary solutions in which the [Cs^+]:[Na^+] and [Cs^+]:[Ca^{2+}] ratios were 1:100. The corresponding distribution coefficients, K_d, for the selective removal of Cs^+ were estimated to be 574 ± 13 and 658 ± 34 cm^3 g^{-1}.

3.3. Kinetics of Sorption of Pb^{2+}, Cd^{2+}, and Cs^+

The removal of Pb^{2+}, Cd^{2+}, and Cs^+ from single metal nitrate solutions by TOB-7 are plotted in Figure 6 and the corresponding pH profiles of the supernatant liquors are shown in Figure 7.

The non-steady-state removal of Pb^{2+} by TOB-7 was found to be 356 ± 8 meq 100 g^{-1} (1.78 mmol g^{-1}, 369 mg g^{-1}) within 24 h, and was accompanied by an increase in pH from 5.8 to 7.2, by virtue of the concomitant release of Na^+ and Ca^{2+} ions from the tobermorite lattice (Figures 6 and 7) [53]. A more modest uptake of 130 ± 12 meq 100 g^{-1} (0.65 mmol g^{-1}, 73 mg g^{-1}) was observed for Cd^{2+} within 24 h with an associated increase in pH from 5.7 to 7.1 (Figures 6 and 7). Pb^{2+} and Cd^{2+} are known to substitute for both inter-layer cations and structural Ca^{2+} ions within the tobermorite lattice, which accounts for the failure to achieve equilibrium within 24 h [18–20,25,32,51,53]. Conversely, the steady state removal of 36 ± 6 meq 100g^{-1} (0.36 mmol g^{-1}, 20 mg g^{-1}) of Cs^+ ions was established within just

30 min (Figure 6). This is typical of the relatively rapid ion exchange involving only the inter-layer cations [18,30,50].

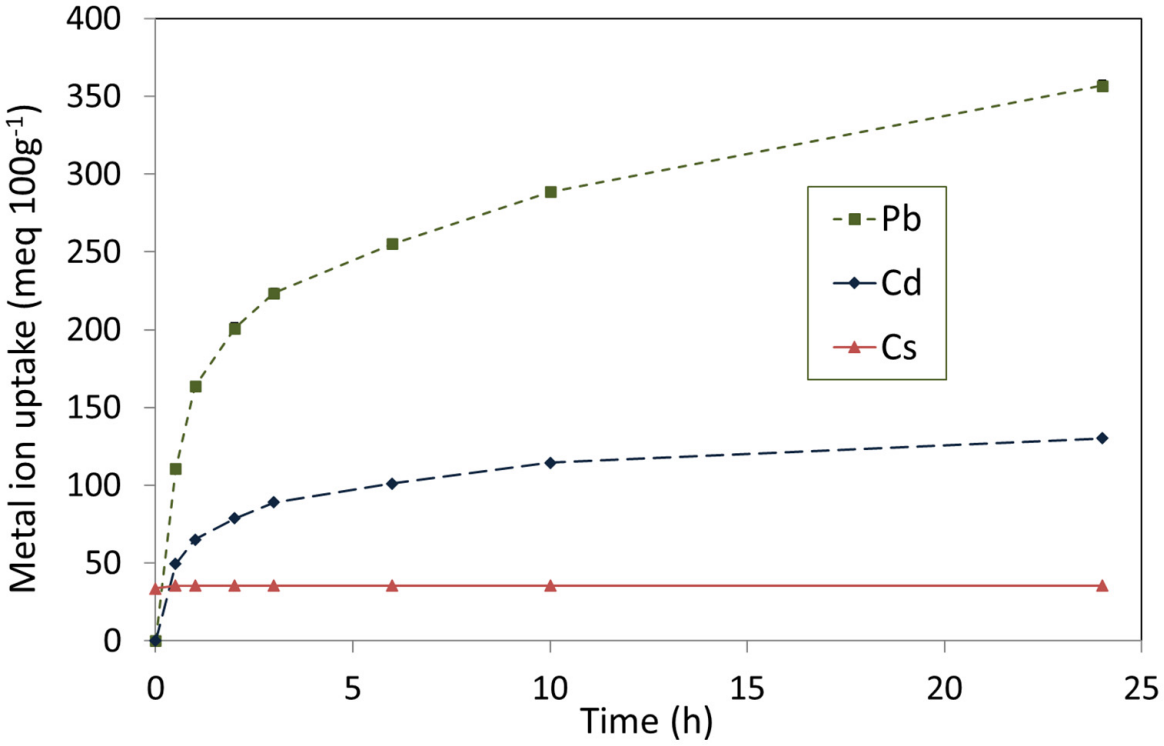

Figure 6. Uptake of Pb^{2+}, Cd^{2+}, and Cs^{+} by the 7-day hydrothermal product.

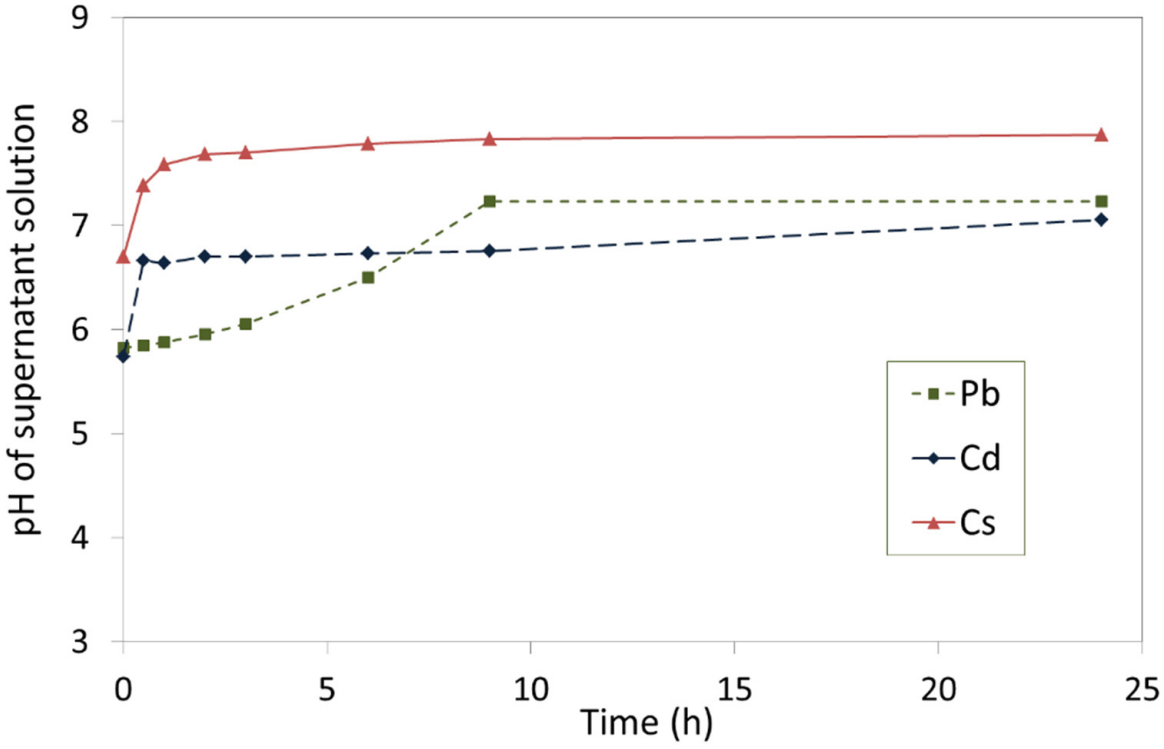

Figure 7. pH of supernatant liquors in contact with the 7-day hydrothermal product (TOB-7).

Experimental data for the uptake of Pb^{2+}, Cd^{2+}, and Cs^{+} by TOB-7 were fitted to the pseudo-first- and pseudo-second-order rate models by least squares regression anal-

ysis [18,20,36]. The apparent rate constants, k_1 and k_2, the calculated maximum uptake values, $q_{calc.}$, and the squares of the linear regression coefficients, R^2, are listed in Table 4.

High correlations between the experimental sorption data for Pb^{2+}, Cd^{2+}, and Cs^+ and the pseudo-second-order kinetic model are evidenced by R^2 values of 0.997, 0.996, and 0.999, respectively (Table 4). Furthermore, the pseudo-second-order kinetic model accurately described the maximum removal of Pb^{2+}, Cd^{2+}, and Cs^+ by TOB-7 to within 7, 5, and 3%, respectively (Table 4).

Table 4. Kinetic parameters for the removal of Pb^{2+}, Cd^{2+}, and Cs^+ from aqueous solutions by the 7-day hydrothermal product (TOB-7).

Kinetic Parameter	Pb	Cd	Cs
Pseudo-first-order model			
k_1 (min^{-1})	2.39×10^{-3}	3.05×10^{-3}	0.102
$q_{calc.}$ (mmol g^{-1})	1.25	2.27	2.66
R^2	0.871	0.912	0.890
Pseudo-second-order model			
k_2 (g $mmol^{-1}$ min^{-1})	0.010	0.027	1.635
$q_{calc.}$ (mol g^{-1})	1.66	0.62	0.35
R^2	0.997	0.996	0.999

4. Discussion

Previous studies have demonstrated that paper recycling ash [25,29,30,36,37,56] and post-consumer container glass [18–21] are suitable feedstocks for the hydrothermal synthesis of 11 Å tobermorite. PRA contains potentially reactive calcium (alumino)silicate phases (e.g., åkermanite, β-dicalcium silicate, anorthite, and gehlenite) that can be exploited in the hydrothermal synthesis of tobermorite, although its molar composition, 0.74 < [Ca]/[Si+Al] < 0.92 and 0.27 < [Al]/[Si+Al] < 0.44, also promotes the formation of katoite [29,36,37,56]. Accordingly, stoichiometric additions of silicate-bearing reagents such as sodium metasilicate or silica have been shown improve the tobermorite yield by appropriately tailoring the constituent ratios to 0.80 < [Ca]/[Si+Al] < 0.85 and 0.0 < [Al]/[Si+Al] < 0.18 [25,36,37].

Irrespective of color, the typical major oxide components of soda-lime-silica container glasses are SiO_2 (70–75 wt%), Na_2O (12–16 wt%), CaO (5–15 wt%), and Al_2O_3 (1–5 wt%), which provide a potentially reactive source of amorphous calcium, silicate, and aluminate species in the following molar ranges: 0.13 < [Ca]/[Si+Al] < 0.23 and 0.015 < [Al]/[Si+Al] < 0.078 [17–21,39,64]. Optimal [Ca]/[Si+Al] ratios for tobermorite formation have been obtained by supplementing the WCG reaction mixture with lime [17–19,21,39] or cement bypass dust (CBD) [20]. Mixtures of WCG and lime require additional alkalinity, such as sodium hydroxide, to depolymerize and dissolve the silicate network [17–19,21,39], whereas CBD possesses sufficient intrinsic alkalinity to activate the glass [20].

In the present study, a novel combination of PRA, WCG, and lime with molar compositional ratios of [Ca]/[Si+Al] = 0.81 and [Al]/[Si+Al] = 0.18 was found, by XRD analysis, to yield a mixed product of 50.3 wt% Al-substituted 11 Å tobermorite, 6.1 wt% katoite, 7.8 wt% calcite, 2.5 wt% portlandite, and 33.3 wt% amorphous material after seven days at 100 °C (Table 2, Figure 3). The discrepancy between the two estimates of crystallinity from XRD analysis (~67 wt%) and ^{29}Si MAS NMR spectroscopy (~75 % of the silicate species) is attributed to the extensive structural disorder of tobermorite and to the formation of a semi-crystalline calcium (alumino)silicate hydrate (C-A-S-H) precursor that is not effectively detected by XRD analysis. In this respect, XRD analysis tends to overestimate the amorphous-content of poorly crystalline calcium silicate hydrate materials synthesized at modest temperatures [13,17].

The Cs^+ cation exchange capacity (CEC) and Cs^+ distribution coefficients (K_d) of the hydrothermal product (TOB-7) from solutions having molar ratios of $[Cs^+]$:$[Na^+]$ or $[Cs^+]$:$[Ca^{2+}]$ equal to 1:100 are compared with those of other bespoke and waste-derived tobermorites in Table 5 [18,27,30,68–73].

Table 5. Cs^+ cation exchange capacity (CEC) and selective Cs^+ distribution coefficients (K_d) from solutions with molar ratios of $[Cs^+]$:$[Na^+]$ or $[Cs^+]$:$[Ca^{2+}]$ equal to 1:100 for various tobermorites.

Tobermorite	Cs^+ CEC (meq 100 g^{-1})	K_d (Cs^+ vs. Na^+) (cm^3 g^{-1})	K_d (Cs^+ vs. Ca^{2+}) (cm^3 g^{-1})
PRA and WCG-derived tobermorite (this study)	59 ± 4	574 ± 13	658 ± 34
Bespoke tobermorites [68]	13–57	-	100–3400
Bespoke tobermorites [69,70]	12–197	120–20370	130–12,850
Bespoke tobermorites (microwave synthesis) [71]	-	621–2648	852–118,589
Bespoke tobermorites [72]	12–77	20–5600	90–15,100
Fly ash-derived tobermorite [73]	7.68–7.75	2265–2374	-
Container glass-derived tobermorite [18]	36.7 ± 1.0	181 ± 53	102 ± 19
Blast furnace slag-derived tobermorites [27]	-	731	514
PRA-derived tobermorite [30]	38.3 ± 4.9	93 ± 9	125 ± 24
Sodium silicate and PRA-derived tobermorites [30]	66.3–85.2	733–5434	708–5538

The displacement of labile inter-layer cations in tobermorites is favored by large, less hydrated ions such as Cs^+ that form inner-sphere complexes with the silicate system [74]. Accordingly, pre-saturation with K^+ and subsequent exchange by Cs^+ has become a widely adopted method for the measurement of the cation exchange capacity of tobermorites [18,27,30,53,68–73]. Superior Cs^+ CECs are generally associated with increasing Al-content, which enhances the negative charge on the silicate lattice, and higher crystallinity gives rise to greater Cs^+ selectivity (i.e., higher K_d values) [30,68–72]. CEC is little affected by crystallinity, whereas low Cs^+ selectivity arises from stacking disorders in the tobermorite lattice causing a lack of uniformity within the inter-layer channels running along the *b*-axis [30].

Bespoke 11 Å tobermorites synthesized from analytical grade reagents are reported to possess Cs^+ CECs in the range 12–197 meq $100g^{-1}$ [68–72], and waste-derived tobermorites generally exhibit lower values between 7.68 and 85.2 meq $100g^{-1}$ [18,27,30,73] (Table 5). The Cs^+ CEC of TOB-7 is greater than those derived from fly ash [73], container glass [18], and unblended PRA [30], although falls short of the value obtained for tobermorite prepared from a combination of PRA, sodium metasilicate, and lime [30] (Table 5).

The Cs^+ selective distribution coefficients, K_d, of bespoke tobermorites for the removal of Cs^+ from Na^+-rich and Ca^{2+}-rich liquors are in the ranges 20–20,370 cm^3 g^{-1} and 90–118,589 cm^3 g^{-1}, respectively (Table 4). In comparison, the respective K_d values of waste-derived tobermorites, 93–5434 cm^3 g^{-1} and 102–5538 cm^3 g^{-1}, are typically inferior to those of bespoke tobermorites (Table 5). The Cs^+ selectivity of TOB-7 is higher than those of tobermorites synthesized exclusively from WCG [18] or PRA [30], comparable to those of blast furnace slag-derived tobermorite [27], and lower than those of tobermorites prepared from fly ash [73] or combinations of PRA, sodium metasilicate, and lime [30] (Table 5).

Overall, the present study confirmed that a stoichiometrically adjusted combination of PRA, WCG, and lime yields a tobermorite product with superior CEC and Cs^+ selectivity to tobermorites derived exclusively from either PRA [30] or WCG [18] under the same reaction conditions (Table 4). The Cs^+ CEC of TOB-7 is acceptable, although its Cs^+ selectivity is comparatively low, indicating that it is not suitable for ion-sieving applications such as the decontamination of $^{137}Cs^+$ from multicomponent liquors.

The batch removals of aqueous Pb^{2+}, Cd^{2+}, and Cs^+ from single metal ion solutions by TOB-7 are compared with those of other bespoke and waste-derived tobermorites in Table 6 [18,20,22,24–27,35,41,42,53,72,75–79]. The ranges of batch uptakes of Pb^{2+} reported for bespoke (0.08–1.85 mmol g^{-1}) [53,74] and waste-derived tobermorites (0.06–2.25 mmol g^{-1}) [18,20,22,24,26,41,42,79] are comparable and do not appear to be related to either crystallinity or Al-content (Table 6). The removal of Cd^{2+} is generally less extensive than that of Pb^{2+} by both bespoke (0.04–1.36 mmol g^{-1}) [53,75] and waste-derived tobermorites (0.111–1.52 mmol g^{-1}) [18,20,22,24,25,42,79], and is similarly unaffected by structural order and composition. Pb^{2+} uptake by TOB-7 appears at the upper end of the

reported distribution for tobermorites, and Cd^{2+} removal by TOB-7 falls within the middle of the range (Table 6).

Table 6. Uptake of Pb^{2+}, Cd^{2+}, and Cs^{+} ions by various tobermorites under batch conditions.

Tobermorite	Pb^{2+}-Uptake (mmol g^{-1})	Cd^{2+}-Uptake (mmol g^{-1})	Cs^{+}-Uptake (mmol g^{-1})
PRA and WCG-derived tobermorite (this study)	1.78 ± 0.04	0.65 ± 0.06	0.36 ± 0.03
Bespoke tobermorites [75]	1.85	0.945	-
Bespoke tobermorites [76]	-	-	0.84
Bespoke tobermorites (microwave synthesis) [77]	-	-	0.6
Bespoke tobermorites [53]	0.08–0.895	0.04–1.36	-
Bespoke tobermorites [72]	-	-	0.564–0.572
Container glass-derived tobermorite [18]	1.66 ± 0.05	0.48 ± 0.01	-
Sodium silicate and PRA-derived tobermorites [25]	-	0.63–1.12	-
Snail shell ash and waste glass-derived tobermorite [22]	0.060	0.111	-
Blast furnace slag-derived tobermorites [27]	-	-	0.112–0.587
Asbestos-bearing disaster waste-derived tobermorite [35]	-	-	0.31–0.51
Fly ash-derived mesoporous tobermorite [26]	1.287	-	-
Alumina-extracted coal fly ash-derived tobermorite [42]	1.636	0.937	-
Alumina-extracted coal fly ash-derived tobermorite [41]	0.850		
Cement bypass dust and glass-derived tobermorite [20]	2.25	1.52	-
Incineration fly ash-derived tobermorite [78]	-	-	0.40
Bottom ash-derived tobermorite/zeolite mixture [79]	0.381	0.196	
Coal ash-derived tobermorite/zeolite mixture [24]	1.98	1.31	-

Pb^{2+} and Cd^{2+} ions are rapidly exchanged for labile inter-layer cations within a few hours, and subsequently also replace structural Ca^{2+} ions within the tobermorite lattice over a longer timeframe. In this respect, the steady state uptake of divalent cations is usually established between 3 and 10 days [18,20,22,24,26,41,42,53,75,79]. In addition to tobermorite, other common components present in waste-derived hydrothermal products such as calcite and portlandite, undoubtedly contribute to the removal of Pb^{2+} and Cd^{2+} via the precipitation of solubility-limiting phases [75], and the amorphous calcium (alumino)silicate gel phase may also enhance the overall sorption capacity.

Irrespective of the various sorption mechanisms, the removal kinetics for both Pb^{2+} and Cd^{2+} by bespoke and waste-derived tobermorites are widely described by the pseudo-second-order model with k_2 values in the respective ranges of 0.00755–0.414 g $mmol^{-1}$ min^{-1} [18,20,24,26] and 0.00259–0.101 g $mmol^{-1}$ min^{-1} [18,20,24], which compare well with the findings of the present study (Table 4).

The extents of batch removal of Cs^{+} ions reported for bespoke tobermorites (0.564–0.84 mmol g^{-1}) [72,76,77] are typically superior to those of their waste-derived counterparts (0.112–0.587 mmol g^{-1}) [27,35,78] (Table 6). As previously stated, Cs^{+} is swiftly exchanged for inter-layer cations and equilibrium is usually achieved within an hour [35]. Cs^{+} batch sorption values tend to be lower than the corresponding CECs measured by Cs^{+} for K^{+} displacement of tobermorites that have been pre-saturated with K^{+} ions [72]. The batch uptake of Cs^{+} by TOB-7 is inferior to those of bespoke tobermorites and compares well with those of other waste-derived samples (Table 6). The associated pseudo-second-order rate constant, 1.635 g $mmol^{-1}$ min^{-1}, was similar to that reported by Wajima (3.5 g $mmol^{-1}$ g^{-1}) for tobermorite synthesized from asbestos-bearing disaster waste [35].

Previous studies have considered the hydrothermal synthesis of tobermorites from a wide range of commercial and industrial waste materials under relatively mild conditions (i.e., 80–125 °C in water or 0.5–4 M $NaOH_{(aq)}$) in order to appraise the reactivity of the feedstock components and to understand the relationship between the structure and properties of the product [16–20,25,29,30,35,36,39,56,73]. Accordingly, the present study investigated the hydrothermal synthesis of Al-substituted tobermorite from a mixture of paper recycling ash (PRA), waste container glass (WCG), and lime at 100 °C in 4 M $NaOH_{(aq)}$.

The findings indicate that this combination of waste materials yields a tobermorite-rich product with superior sorption properties to tobermorites derived from the individual PRA or WCG feedstocks [18,30] (Tables 5 and 6). The uptake of divalent cations depends little on crystallinity and Al-content, and in this respect, the facile one-pot synthesis successfully produces a tobermorite-rich product with attractive sorption characteristics for Pb^{2+} and Cd^{2+} (Figure 6 and Table 6).

Modest reaction temperatures offer the possibility of hydrothermally synthesizing materials by garnering heat generated from other higher-temperature industrial processes [80]. In this respect, some of the energy recovered from the combustion of the paper recycling sludge could be used directly, in situ, to convert the resulting ash into value-added hydrothermal products.

The yield, crystallinity, CEC, and Cs^+ selectivity of the PRA and WCG-derived tobermorites could, hypothetically, be improved by lowering the [Al]/[Si+Al] ratio of the mixture to eliminate katoite, and by increasing the reaction temperature up to ~200 °C [7]. A reduction in $NaOH_{(aq)}$ concentration may also improve the structural integrity of the resulting tobermorite lattice [30]. In addition, further work to consider the production of autoclaved construction and insulating materials, based upon tobermorite and xonotlite [13], from combinations of PRA and WCG is suggested.

5. Conclusions

The present study reports the facile one-pot hydrothermal synthesis of Al-substituted tobermorite from a combination of paper recycling ash (PRA), waste container glass (WCG), and lime, with compositional ratios of [Ca]/[Si+Al] = 0.81 and [Al]/[Si+Al] = 0.18, at 100 °C in 4 M $NaOH_{(aq)}$. The åkermanite, β-dicalcium silicate, and anorthite constituents of PRA were consumed within one day, and gehlenite had completely reacted after one week to yield a mixed product of 50.3 wt% Al-substituted 11 Å tobermorite, 6.1 wt% katoite, 7.8 wt% calcite, 2.5 wt% portlandite, and 33.3 wt% X-ray amorphous material. ^{29}Si magic angle spinning nuclear magnetic resonance spectroscopy indicated that a calcium (alumino)silicate gel phase accounted for approximately 25% of the silicate species within the sample. The Cs^+ cation exchange capacity, selective Cs^+ distribution coefficients, and batch uptakes of aqueous Pb^{2+}, Cd^{2+}, and Cs^+ by the hydrothermal product compared favorably with those of other waste-derived tobermorites reported in the literature. Tobermorite yield, crystallinity, and sorption characteristics could potentially be improved by adjusting the reactant stoichiometry and hydrothermal processing parameters.

Author Contributions: Conceptualization, N.J.C.; Methodology, N.J.C. and A.P.H.; Software, H.M. and Q.L.; Validation, N.J.C., A.A.C. and A.P.H.; Formal analysis, N.J.C., A.A.C., A.P.H., H.M. and Q.L.; Investigation, N.J.C., A.A.C. and A.P.H.; Resources, N.J.C., A.P.H., H.M. and Q.L.; Data curation, N.J.C.; Writing—original draft preparation, N.J.C.; Writing—review and editing, A.A.C., A.P.H. and Q.L.; Visualization, N.J.C., A.A.C., A.P.H. and Q.L.; Supervision, N.J.C.; Project administration, N.J.C.; Funding acquisition, N.J.C. All authors have read and agreed to the published version of the manuscript.

Funding: This research received no external funding.

Institutional Review Board Statement: Not applicable.

Informed Consent Statement: Not applicable.

Data Availability Statement: Data are available on request from the corresponding author.

Acknowledgments: The authors acknowledge, with gratitude, the technical support provided by their late friend and colleague, Ian Slipper, in the collection of the XRD and SEM data.

Conflicts of Interest: The authors declare no conflict of interest.

Appendix A. Example of XRD Phase Identification and Refinement

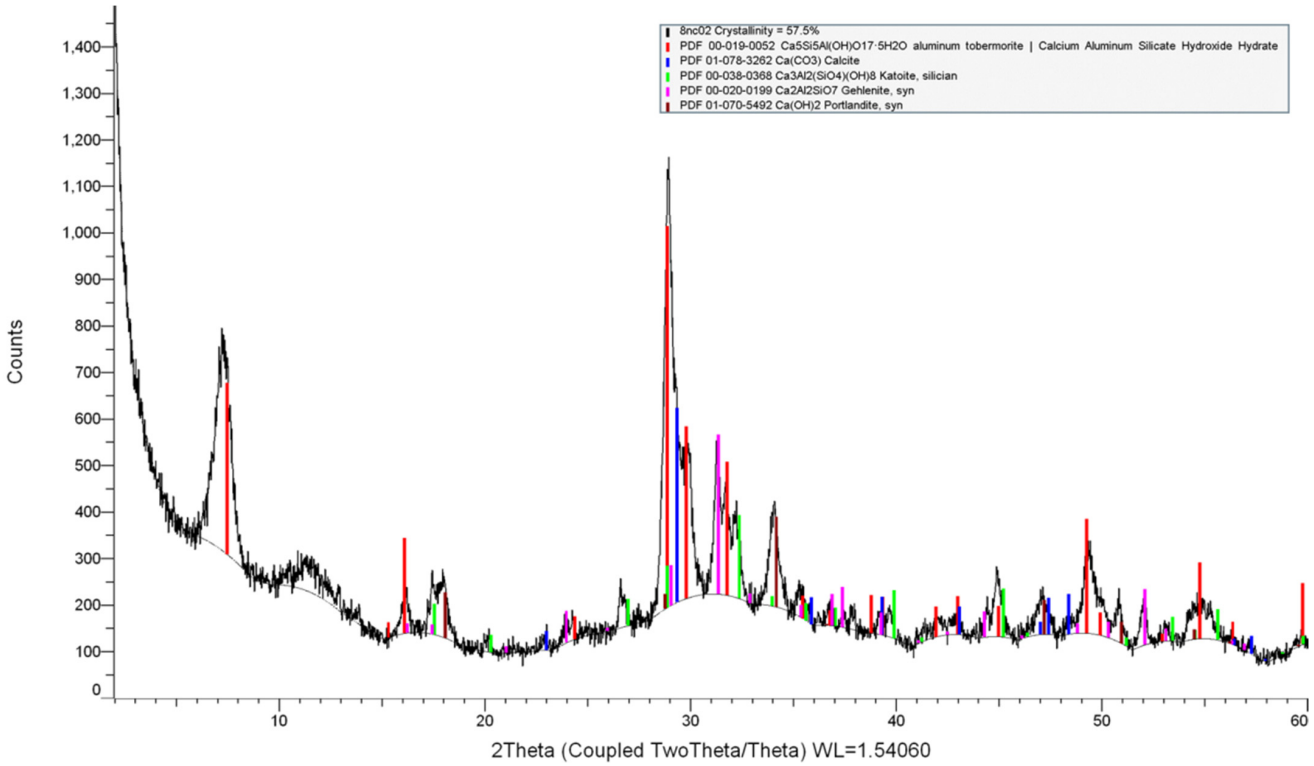

Figure A1. XRD pattern of TOB-2 showing the identification of reflections from 11 Å tobermorite (PDF® 00-019-0052, red lines), katoite (PDF® 00-038-0368, green lines), portlandite (PDF® 01-070-5492, brown lines), calcite (PDF® 01-078-3262, blue lines), and gehlenite (PDF 00-020-0199, pink lines).

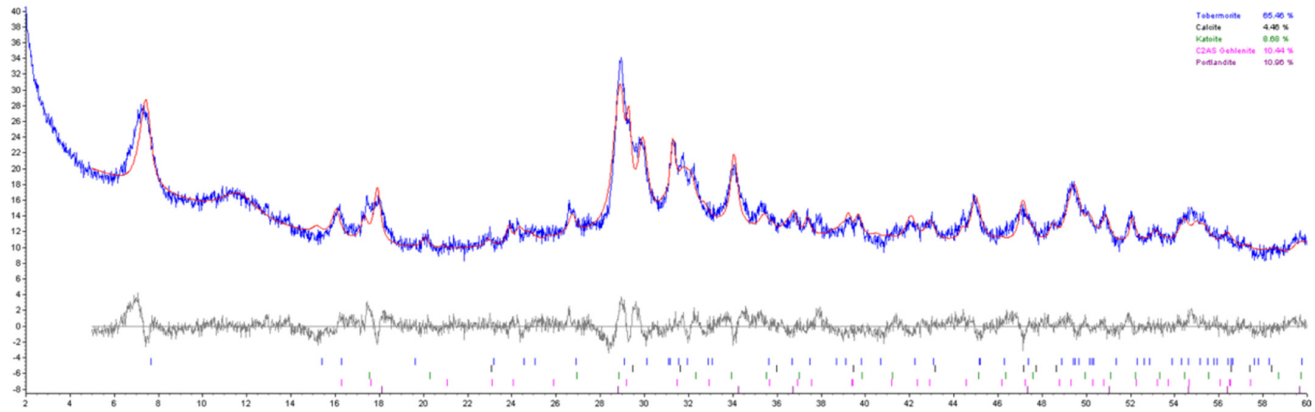

Figure A2. XRD pattern, calculated pattern, and residual for TOB-2.

References

1. Merlino, S.; Bonaccorsi, E.; Armbruster, T. The real structure of tobermorite 11 Å: Normal and anomalous forms, OD character and polytypic modifications. *Eur. J. Mineral.* **2001**, *13*, 577–590. [CrossRef]
2. Fan, J.; Cao, D.; Jing, Z.; Zhang, Y.; Pu, L.; Jing, Y. Synthesis and microstructure analysis of autoclaved aerated concrete with carbide slag addition. *J. Wuhan Univ. Technol. Mater. Sci. Ed.* **2014**, *29*, 1005–1010. [CrossRef]
3. Galvánková, L.; Másilko, J.; Solný, T.; Štěpánková, E. Tobermorite synthesis under hydrothermal conditions. *Procedia Eng.* **2016**, *151*, 100–107. [CrossRef]
4. Martin, S.I. Synthesis of tobermorite: A cement phase expected under repository conditions. In Proceedings of the International High-Level Radioactive Waste Management Conference: Progress toward Understanding, Las Vegas, NV, USA, 1–5 May 1995.
5. Atkinson, A.; Harris, A.W.; Hearne, J.A. *Hydrothermal Alteration and Ageing of Synthetic Calcium Silicate Hydrate Gels, UK Nirex Report NSS/R374*; UK Nirex Ltd.: Oxfordshire, UK, 1995.

6. Jackson, M.D.; Mulcahy, S.R.; Chen, H.; Li, Y.; Li, Q.; Cappelletti, P.; Wenk, H.-R. Phillipsite and Al-tobermorite mineral cements produced through low-temperature water-rock reactions in Roman marine concrete. *Am. Min.* **2017**, *102*, 1435–1450. [CrossRef]
7. Qu, X.; Zhao, Z.; Zhao, X. Microstructure and characterization of aluminum incorporated calcium silicate hydrates (C-S-H) under hydrothermal conditions. *RSC Adv.* **2018**, *8*, 28198. [CrossRef] [PubMed]
8. Hurt, A.P.; Getti, G.; Coleman, N.J. Bioactivity and biocompatibility of a chitosan-tobermorite composite membrane for guided tissue regeneration. *Int. J. Biol. Macromol.* **2014**, *64*, 11–16. [CrossRef]
9. Coleman, N.J. Aspects of the in vitro bioactivity and antimicrobial properties of Ag^{+}-and Zn^{2+}-exchanged 11 Å tobermorites. *J. Mater. Sci. Mater. Med.* **2009**, *20*, 1347–1355. [CrossRef]
10. Maeda, H.; Tamura, T.; Kasuga, T. Improving the biocompatibility of tobermorite by incorporating calcium phosphate clusters. *Biomed. Mater. Eng.* **2017**, *28*, 31–36. [CrossRef]
11. Wu, Y.; Pan, X.; Li, Q.; Yu, H. Crystallization and phase transition of tobermorite synthesized by hydrothermal reaction from dicalcium silicate. *Int. J. Appl. Ceram. Technol.* **2020**, *17*, 1213–1223. [CrossRef]
12. Siauciunas, R.; Smalakys, G.; Dambrauskas, T. Porosity of calcium silicate hydrates synthesized from natural rocks. *Materials* **2021**, *14*, 5592. [CrossRef]
13. Siauciunas, R.; Smalakys, G.; Eisinas, A.; Prichockiene, E. Synthesis of high crystallinity 1.13 nm tobermorite and xonotlite from natural rocks, their properties and application for heat-resistant products. *Materials* **2022**, *15*, 3474. [CrossRef] [PubMed]
14. Youssef, H.; Ibrahim, D.; Komarneni, S.; Mackenzie, K.J.D. Synthesis of 11 Å Al-substituted tobermorite from trachyte rock by hydrothermal treatment. *Ceram. Int.* **2010**, *36*, 203–209. [CrossRef]
15. Liu, S.; Qi, X.; Han, C.; Liu, J.; Sheng, X.; Li, H.; Luo, A.; Li, J. Novel nano-submicron mineral-based soil conditioner for sustainable agricultural development. *J. Clean. Prod.* **2017**, *149*, 896–903. [CrossRef]
16. Malferrari, D.; Bernini, F.; Di Giuseppe, D.; Scognamiglio, V.; Gualtieri, A.F. Al-substituted tobermorites: An effective cation exchanger synthesized from "end-of-waste" materials. *ACS Omega* **2022**, *7*, 1694–1702. [CrossRef]
17. Rahman, H.; Li, Q.; Coleman, N.J. Waste glass-derived tobermorite carriers for Ag^{+} and Zn^{2+} ions. *J. Compos. Sci.* **2022**, *6*, 52. [CrossRef]
18. Coleman, N.J. 11 Å tobermorite ion exchanger from recycled container glass. *Int. J. Environ. Waste Manag.* **2011**, *8*, 366–382. [CrossRef]
19. Coleman, N.J.; Li, Q.; Raza, A. Synthesis, structure and performance of calcium silicate ion exchangers from recycled container glass. *Physicochem. Probl. Miner. Process.* **2014**, *50*, 5–16. [CrossRef]
20. Coleman, N.J.; Trice, C.J.; Nicholson, J.W. 11 Å tobermorite from cement bypass dust and waste container glass: A feasibility study. *Int. J. Miner. Process.* **2009**, *93*, 73–78. [CrossRef]
21. Majdinasab, A.; Yuan, Q. Synthesis of Al-substituted 11Å tobermorite using waste glass cullet: A study on the microstructure. *Mater. Chem. Phys.* **2020**, *250*, 123069. [CrossRef]
22. Lamidi, Y.D.; Owoeye, S.S.; Abegunde, S.M. Removal of heavy metals (Cd and Pb) from aqueous solutions by adsorption using synthetic tobermorite prepared from bio-municipal wastes as adsorbent. *Glob. J. Eng. Technol. Adv.* **2021**, *6*, 076–090. [CrossRef]
23. Wang, S.; Peng, X.; Tang, L.; Zeng, L.; Lan, C. Influence of inorganic admixtures on the 11 Å-tobermorite formation prepared from steel slags: XRD and FTIR analysis. *Con. Build. Mater.* **2014**, *60*, 42–47. [CrossRef]
24. Li, G.; Li, M.; Zhang, X.; Cao, P.; Jiang, H.; Luo, J.; Jiang, T. Hydrothermal synthesis of zeolites-calcium silicate hydrate composite from coal fly ash with co-activation of $Ca(OH)_2$-NaOH for aqueous heavy metals removal. *Int. J. Min. Sci. Technol.* **2022**, *in press*. [CrossRef]
25. Coleman, N.J. Interactions of Cd (II) with waste-derived 11 Å tobermorites. *Sep. Purif. Technol.* **2006**, *48*, 62–70. [CrossRef]
26. Wang, Z.; Xu, L.; Wu, D.; Zheng, S. Hydrothermal synthesis of mesoporous tobermorite from fly ash with enhanced removal performance towards Pb^{2+} from wastewater. *Colloids Surf. A Physicochem. Eng. Asp.* **2022**, *632*, 127775. [CrossRef]
27. Tsutsumi, T.; Nishimoto, S.; Kameshima, Y.; Miyake, M. Hydrothermal preparation of tobermorite from blast furnace slag for Cs^{+} and Sr^{2+} sorption. *J. Hazard. Mater.* **2014**, *266*, 174–181. [CrossRef]
28. Reinik, J.; Heinmaa, I.; Kirso, U.; Kallaste, T.; Ritamäki, J.; Boström, D.; Pongrácz, E.; Huuhtanen, M.; Larsson, W.; Keiski, R.; et al. Alkaline modified oil shale fly ash: Optimal synthesis conditions and preliminary tests on CO_2 adsorption. *J. Hazard. Mater.* **2011**, *196*, 180–186. [CrossRef]
29. Coleman, N.J.; Brassington, D.S. Synthesis of Al-substituted 11 Å tobermorite from newsprint recycling residue: A feasibility study. *Mater. Res. Bull.* **2003**, *38*, 485–497. [CrossRef]
30. Coleman, N.J. Synthesis, structure and ion exchange properties of 11 Å tobermorites from newsprint recycling residue. *Mater. Res. Bull.* **2005**, *40*, 2000–2013. [CrossRef]
31. Cao, P.; Li, G.; Luo, J.; Rao, M.; Jiang, H.; Peng, Z.; Jiang, T. Alkali-reinforced hydrothermal synthesis of lathy tobermorite fibers using mixture of coal fly ash and lime. *Constr. Build. Mater.* **2020**, *238*, 117655. [CrossRef]
32. Zou, J.; Guo, C.; Zhou, X.; Sun, Y.; Yang, Z. Sorption capacity and mechanism of Cr^{3+} on tobermorite derived from fly ash acid residue and carbide slag. *Colloids Surf. A Physicochem. Eng. Asp.* **2018**, *538*, 825–833. [CrossRef]
33. Luo, F.; Wei, C.; Xue, B.; Wang, S.; Jiang, Y. Dynamic hydrothermal synthesis of Al-substituted 11 Å tobermorite from solid waste fly ash residue-extracted Al_2O_3. *Res. Chem. Intermed.* **2013**, *39*, 693–705. [CrossRef]
34. Smalakys, G.; Siauciunas, R. The hydrothermal synthesis of 1.13 nm tobermorite from granite sawing powder waste. *Ceram. Silik.* **2020**, *64*, 239–248. [CrossRef]

35. Wajima, T. Synthesis of tobermorite from the ash after treatment of asbesto-containing disaster waste, and its removal ability of Cs(I) from aqueous solution. *Eng. J.* **2016**, *20*, 79–91. [CrossRef]
36. Coleman, N.J.; Brassington, D.S.; Raza, A.; Mendham, A.P. Sorption of Co^{2+} and Sr^{2+} by waste-derived 11 Å tobermorite. *Waste Manag.* **2006**, *26*, 260–267. [CrossRef] [PubMed]
37. Miao, J.; Zhu, W.; Liang Yue, L.; Jing, Z. Reutilizing paper mill sludge as humidity regulating material by hydrothermal solidifying. *Waste Biomass Valorization* **2022**, *in press*. [CrossRef]
38. Yang, Z.; Zhang, D.; Jiao, Y.; Fang, C.; Kang, D.; Yan, C.; Zhang, J. Crystal evolution of calcium silicate minerals synthesized by calcium silicon slag and silica fume with increase of hydrothermal synthesis temperature. *Materials* **2022**, *15*, 1620. [CrossRef] [PubMed]
39. Elmes, V.K.; Hurt, A.P.; Coleman, N.J. Mixed-phase ion-exchangers from waste amber container glass. *Materials* **2021**, *14*, 4887. [CrossRef]
40. Zhang, J.; Xu, Q.; Wang, H.; Li, S. Preparation of hydrothermally solidified materials from waste cathode ray tube panel glass for construction applications. *Environ. Sci. Pollut. Res.* **2022**, *in press*. [CrossRef]
41. Yang, J.; Sun, H.; Peng, T.; Zeng, L.; Zhou, X. Mild hydrothermal synthesis of 11Å-TA from alumina extracted coal fly ash and its application in water adsorption of heavy metal ions (Cu(II) and Pb(II)). *Int. J. Environ. Res. Public Health* **2022**, *19*, 616. [CrossRef]
42. Wang, Z.; Huang, Z.; Zheng, S.; Wu, D.; Cai, W. Effective removal of Pb^{2+} and Cd^{2+} from wastewater by mesoporous tobermorite synthesized from alumina-extracted fly ash. *Desalination Water Treat.* **2021**, *235*, 209–220. [CrossRef]
43. Tian, H.; Stephan, D.; Lothenbach, B.; Lehmann, C. Influence of foreign ions on calcium silicate hydrate under hydrothermal conditions: A review. *Constr. Build. Mater.* **2020**, *301*, 124071. [CrossRef]
44. Wang, Z.; Ma, S.; Zheng, S.; Wang, X. Incorporation of Al and Na in hydrothermally synthesized tobermorite. *J. Am. Ceram. Soc.* **2017**, *100*, 792–799. [CrossRef]
45. Zhao, Z.; Wei, J.; Li, F.; Qu, X.; Shi, L.; Zhang, H.; Yu, Q. Synthesis, characterization and hexavalent chromium adsorption characteristics of aluminum- and sucrose-incorporated tobermorite. *Materials* **2017**, *10*, 597. [CrossRef] [PubMed]
46. Mostafa, N.Y.; Kishar, E.A.; Abo-El-Enein, S.A. FTIR study and cation exchange capacity of Fe^{3+}- and Mg^{2+}-substituted calcium silicate hydrates. *J. Alloys Compd.* **2009**, *473*, 538–542. [CrossRef]
47. Mostafa, N.Y.; Shaltout, A.A.; Omarb, H.; Abo-El-Enein, S.A. Hydrothermal synthesis and characterization of aluminium and sulfate substituted 1.1 nm tobermorites. *J. Alloys Compd.* **2009**, *467*, 332–337. [CrossRef]
48. Kamei, S.; Ihara, T.; Ouchi, T.; Uzawa, M.; Machinaga, O. A novel synthesis of phosphorus-substituted tobermorite with calcium silicate hydrate. *J. Ceram. Soc. Jpn.* **2014**, *122*, 664–667. [CrossRef]
49. Ferreira, A.; Ananias, D.; Carlos, L.D.; Morais, C.M.; Rocha, J. Novel microporous lanthanide silicates with tobermorite-like structure. *J. Am. Chem. Soc.* **2003**, *125*, 14573–14579. [CrossRef]
50. Shrivastava, O.P.; Shrivastava, R. Study on selective sorption of Cs-137 on Al-substituted calcium silicate hydroxy hydrate. *J. Indian Chem. Soc.* **2001**, *78*, 392–394.
51. Mandaliev, P.; Wieland, E.; Dähn, R.; Tits, J.; Churakov, S.V.; Zaharko, O. Mechanisms of Nd(III) uptake by 11 Å tobermorite and xonotlite. *Appl. Geochem.* **2010**, *25*, 763–777. [CrossRef]
52. Komarneni, S.; Roy, R.; Roy, D.M. Pseudomorphism in xonotlite and tobermorite with Co^{2+} and Ni^{2+} exchange for Ca^{2+} at 25 °C. *Cem. Concr. Res.* **1986**, *16*, 47–58. [CrossRef]
53. Al-Wakeel, E.I.; El-Korashy, S.A.; El-Hemaly, S.A.; Rizk, M.A. Divalent ion uptake of heavy metal cations by (aluminum + alkali metals)—Substituted synthetic 1.1 nm-tobermorites. *J. Mater. Sci.* **2001**, *36*, 2405–2415. [CrossRef]
54. European Paper Recycling Council. Monitoring Report 2020. Available online: https://www.cepi.org/wp-content/uploads/2021/07/WEB-PAGES_EPRC-Monitoring-Report-2020_20210716.pdf (accessed on 8 June 2022).
55. Bousios, S.; Worrell, E. Towards a Multiple Input-Multiple Output paper mill: Opportunities for alternative raw materials and sidestream valorisation in the paper and board industry. *Resour. Conserv. Recycl.* **2017**, *125*, 218–232. [CrossRef]
56. Wajima, T. Chemical conversion of paper sludge ash into cation exchanger via acid leaching. *J. Ion Exch.* **2022**, *33*, 27–31. [CrossRef]
57. Jiang, Y.; Ling, T.C.; Mo, K.H.; Shi, C. A critical review of waste glass powder—Multiple roles of utilization in cement-based materials and construction products. *J. Environ. Manag.* **2019**, *242*, 440–449. [CrossRef] [PubMed]
58. Conradt, R. Prospects and physical limits of processes and technologies in glass melting. *J. Asian Ceram. Soc.* **2019**, *7*, 377–396. [CrossRef]
59. Majdinasab, A.; Yuan, Q. Post-consumer cullet and potential engineering applications in North America. *Resour. Concerv. Recy.* **2019**, *147*, 1–9. [CrossRef]
60. Silva, R.V.; de Brito, J.; Lye, C.Q.; Dhir, R.K. The role of glass waste in the production of ceramic-based products and other applications: A review. *J. Clean. Prod.* **2017**, *167*, 346–364. [CrossRef]
61. Ayala Valderrama, D.M.; Gómez Cuaspud, J.A.; Roether, J.A.; Boccaccini, A.R. Development and characterization of glass-ceramics from combinations of slag, fly ash, and glass cullet without adding nucleating agents. *Materials* **2019**, *12*, 2032. [CrossRef]
62. Bobirică, C.; Shim, J.-H.; Park, J.-Y. Leaching behavior of fly ash-waste glass and fly ash-slag-waste glass-based geopolymers. *Ceram. Int.* **2018**, *44*, 5886–5893. [CrossRef]
63. Giro-Paloma, J.; Barreneche, C.; Maldonado-Alameda, A.; Royo, M.; Formosa, J.; Inés Fernández, A.; Chimenos, J.M. Alkali-activated cements for TES materials in buildings' envelops formulated with glass cullet recycling waste and microencapsulated phase change materials. *Materials* **2019**, *12*, 2144. [CrossRef]

64. Taylor, J.H.; Elmes, V.E.; Hurt, A.P.; Coleman, N.J. Synthesis of feldspathoids and zeolite K–F from waste amber container glass. *Mater. Chem. Phys.* **2020**, *246*, 122805. [CrossRef]
65. Elmes, V.E.; Mendham, A.P.; Coleman, N.J. A waste-derived lithium metasilicate basic catalyst. *MATEC Web Conf.* **2017**, *109*, 03004. [CrossRef]
66. Coelho, A.A. TOPAS and TOPAS-Academic: An optimization program integrating computer algebra and crystallographic objects written in C++. *J. Appl. Crystallogr.* **2018**, *51*, 210–218. [CrossRef]
67. Andersen, M.D.; Hans, J.; Jakobsen, H.J.; Skibsted, J. Characterization of white Portland cement hydration and the C-S-H structure in the presence of sodium aluminate by ^{27}Al and ^{29}Si MAS NMR spectroscopy. *Cem. Concr. Res.* **2004**, *34*, 857–868. [CrossRef]
68. Komarneni, S.; Roy, D.M.; Roy, R. Al-substituted tobermorite: Shows cation exchange. *Cem. Concr. Res.* **1982**, *12*, 773–780. [CrossRef]
69. Komarneni, S.; Roy, D.M. Tobermorites: A new family of cation exchangers. *Science* **1983**, *221*, 647–648. [CrossRef] [PubMed]
70. Komarneni, S.; Roy, D.M. New tobermorite cation exchangers. *J. Mater. Sci.* **1985**, *20*, 2930–2936. [CrossRef]
71. Komarneni, S.; Komarneni, J.S.; Newalkar, B.; Stout, S. Microwave-hydrothermal synthesis of Al-substituted tobermorite from zeolites. *Mater. Res. Bull.* **2002**, *37*, 1025–1032. [CrossRef]
72. Komarneni, S.; Breval, E.; Miyake, M.; Roy, R. Cation-exchange properties of (Al + Na)-substituted synthetic tobermorites. *Clays Clay Miner.* **1987**, *35*, 385–390. [CrossRef]
73. Ma, W.; Brown, P.W.; Komarneni, S. Characterization and cation exchange properties of zeolite synthesized from fly ashes. *J. Mater. Res.* **1998**, *13*, 3–7. [CrossRef]
74. Bu, J.; Gonzalez Teresa, R.; Brown, K.G.; Sanchez, F. Adsorption mechanisms of cesium at calcium-silicate-hydrate surfaces using molecular dynamics simulations. *J. Nucl. Mater.* **2019**, *515*, 35–51. [CrossRef]
75. Komarneni, S.; Breval, E.; Roy, D.M.; Roy, R. Reactions of some calcium silicates with metal cations. *Cem. Concr. Res.* **1988**, *18*, 204–220. [CrossRef]
76. Miyake, M.; Komarneni, S.; Roy, R. Kinetics equilibria and thermodynamics of ion exchange in substituted tobermorites. *Mater. Res. Bull.* **1989**, *24*, 311–320. [CrossRef]
77. Miyake, M.; Niiya, S.; Matsuda, M. Microwave-assisted Al-substituted tobermorite synthesis. *J. Mater. Res.* **2000**, *15*, 850–853. [CrossRef]
78. Yao, Z.; Tamura, C.; Kusano, F.; Matsuda, M.; Miyake, M. Resource recovery of waste incineration fly ash: Synthesis of tobermorite as an ion exchanger. *J. Mater. Res.* **1999**, *14*, 4437–4442. [CrossRef]
79. Chiang, Y.W.; Ghyselbrecht, K.; Santos, R.M.; Meesschaert, B.; Martens, J.A. Synthesis of zeolitic-type adsorbent material from municipal solid waste incinerator bottom ash and its application in heavy metal adsorption. *Catal. Today* **2012**, *190*, 23–30. [CrossRef]
80. Jouhara, H.; Khordehgah, N.; Almahmoud, S.; Delpech, B.; Chauhan, A.; Tassou, S.A. Waste heat recovery technologies and applications. *Therm. Sci. Eng. Prog.* **2018**, *6*, 268–289. [CrossRef]